CHEMICAL PROBLEMS OF THE DEVELOPMENT OF NEW MATERIALS AND TECHNOLOGIES
Minsk 2003

M. Ivanovskaya,
D. Kotsikau, D. Orlik

GAS-SENSITIVE PROPERTIES OF OXIDE SYSTEMS BASED ON In_2O_3 AND SnO_2 OBTAINED BY SOL-GEL TECHNOLOGY

INTRODUCTION

The results of investigations of gas-sensitive behavior and structural peculiarities of ultra-dispersed semiconducting metal oxides, performed by the group of Thin Film Laboratory in the latest years have been summarized in the paper. The distinctive feature of this kind of investigations as compared to other institutions is that gas-sensitive oxide layers in form of ceramics, thin- and thick films were prepared by using colloid solutions of metal hydroxides stabilized by different additives like organic and inorganic acids, binding and surface active agents. Paper overview devoted to the methods of oxide system synthesis and the regularities of their formation is given in [1].

1. EXPERIMENTAL

Oxides and oxide nanocomposites have been obtained by co-precipitation of metal hydroxides followed by their conversion into colloid solutions and thermal treatment at different temperatures. Thin film and ceramic sensors were fabricated by using colloid solutions. Powders were used for performing certain structural studies and for the fabrication of thick film sensors.

Structural features of powder and film samples were studied by XRD, ESR, Mossbauer spectroscopy, TEM, SEM, XPS, IR and Optical spectroscopies.

Gas-sensitive properties of ceramic and thin film sensors were investigated. Construction of the indicated sensors is presented in the Fig. 1. Forming procedures of ceramic and thin film sensors have been described elsewhere [2–4]. Response (ΔU) of ceramic sensors was determined as $\Delta U = U_{air} - U_{gas}$, where U_{air}, U_{gas} represent sensor voltages at constant current in air and gas ambient, correspondingly. Sensitivity (S) of thin film sensors at the detection of reducing and oxidizing gases was determined as $S = R_{air}/R_{gas}$ and $S = R_{gas}/R_{air}$, correspondingly, where R_{air}, R_{gas} are sensitive layer resistances in air and gas ambient.

2. STRUCTURAL PECULIARITIES OF OXIDE SYSTEMS OBTAINED BY SOL-GEL TECHNOLOGY

Oxide systems prepared by sol-gel technology demonstrate certain structural peculiarities. They are characterized by high dispersity and defectiveness, formation of metastable phases, stabilization of ions in unusual oxidation state.

Particle average size for simple oxides does not exceed 10 nm after annealing at 300 °C. In the case of thin films, high dispersity preserves up to 800 °C (Table 1).

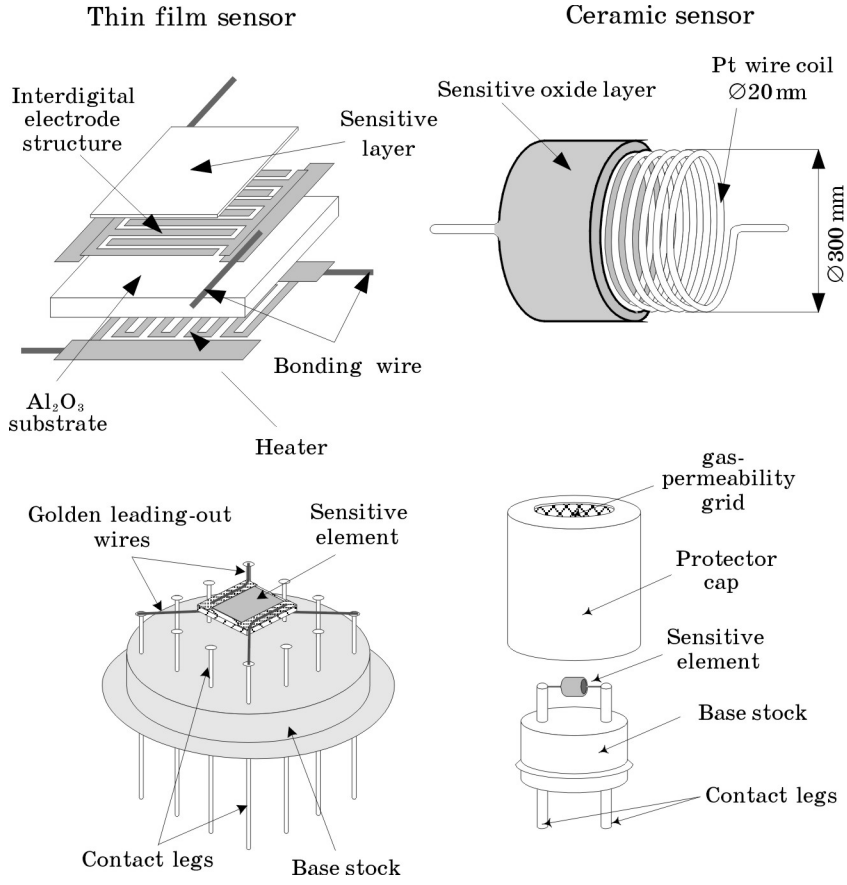

Fig. 1. Construction of thin film- and ceramic sensors

Stabilization of various metastable defects is also typical of oxide systems prepared by sol-gel method. The most characteristic structural defects for oxides obtained by thermal treatment of xerogels are shown in the Table 2.

Table 1

Average grain size of simple oxides annealed at different temperatures

Sample Characteristics	Grain Size, nm						
	100 °C	300 °C	400 °C	500 °C	600 °C	800 °C	1100 °C
In_2O_3 (film, HNO_3)		4	6		12	25	
SnO_2 (film, oleic acid)	2	2		5		10	35
SnO_2 (powder, oleic acid,)	2	4	10	30		150	150
SnO_2 (powder, w/o stabilizer)	2	3	4	10		50	120
SnO_2 (powder, HNO_3)	2			6	7	40	
TiO_2 (powder, CH_3COOH)	4	6		30	35	200	
TiO_2 (film, w/o stabilizer)	7	7		10	12	75	
α-Fe_2O_3 (powder, HNO_3)	2	2	5	15		75	
γ-Fe_2O_3 (powder, HNO_3)		6 (γ)		10 (γ) 35 (α)		45 (α)	

Table 2

The most characteristic defects of oxide structures obtained by thermal treatment of xerogels

Oxide	Structural Defects	Methods of Investigation
SnO_{2-x}	V_O^-, $Sn^{(4-\delta)+}$–$V_O^{\delta-}$, Sn^{2+}, Sn^{3+}, *F*-centers	ESR; Mössbauer spectroscopy
$In2O_{3-x}$	In^{2+}, *F*-centers	ESR, XPS
TiO_{2-x}	Ti^{3+} (regular and interstitial), Ti_2^{7+}, *F*-centers	ESR, XPS
MoO_3	5- and 6-fold coordinated Mo^{5+}, O^-, *F*-centers	ESR, XPS, Optical spectroscopy

Thus, the formation of significant amounts of single charged oxygen vacancies in slightly different coordination neighborhood is found in sol-gel obtained SnO_2 by ESR [5]. According to the results of Mössbauer spectroscopy, partial reduction of Sn^{4+} ions, liading to the formation of Sn^{3+} and Sn^{2+} intermediate oxidation states, takes place in SnO_2 and SnO_2–Pd films [6]. Probably, this process is caused by charge transfer from oxygen vacancies to tin ions. For ^{119}Sn nuclei correlation between chemical shift value and tin oxidation state occurs. Under the growth of s-electron density at tin nucleus chemical shift is positive, as we observed for sol-gel synthesized and annealed SnO_2. *F*-centers and In^{2+} ions in two types of coordination neighborhood are found in In_2O_3 after annealing in air [7, 8]. Interstitial and regular Ti^{3+} ions and Ti_2^{7+} dimers, which are characteristic of partially reduced Ti_nO_{2n-1} oxide phases, are formed [9]. Mo^{5+} centers in different coordination are stabilized in MoO_3 under annealing in air [10].

As it follows from ESR study, capturing of unpaired electrons by several nuclei simultaneously that results in the formation of complex defect is characteristic of most of non-stoichiometric oxides. Local charge compensation as well as bulk one accompanying by the formation of paramagnetic defects is possible. The data available indicate that there are common regularities in distribution of electronic density within crystal lattice, that depends on cation nature. For most of cations the possibility of electron capture (a) can be expressed as $a = z/r^2$, where z – actual cation charge, r – cation radius. Ionic cation radiuses and ionization po-

tentials of the studied metals are listed in the Tables 3, 4. From the data reported it follows that the efficiency of electron capture by cation rises within the row: $In^{3+}<Zr^{4+}<Sn^{4+}<Fe^{3+}<Ti^{4+}<Mo^{6+}$.

Table 3

Ionic radiuses of some metal cations

Cation	In^{3+}	Zr^{4+}	Sn^{4+}	Fe^{3+}	Ti^{4+}	Mo^{6+}
r, Å (cn 4)	0.76	0.73	0.69	0.63	0.56	0.55
r, Å (cn 6)	0.94	0.86	0.83	0.79	0.75	0.75

Table 4

Ionization potential of some metal cations

Transition	Ionization Potential, *eV*
$In^{2+} \rightarrow In^{3+}$	28.035
$Al^{2+} \rightarrow Al^{3+}$	28.447
$Fe^{2+} \rightarrow Fe^{3+}$	30.650
$Zr^{3+} \rightarrow Zr^{4+}$	34.336
$Ni^{2+} \rightarrow Ni^{3+}$	35.165
$Sn^{3+} \rightarrow Sn^{4+}$	40.734
$Ti^{3+} \rightarrow Ti^{4+}$	43.265
$Mo^{5+} \rightarrow Mo^{6+}$	68.402

The formation of metastable at r.t. oxide phases (*H*-In_2O_3, *M*-In_2O_3, *H*-MoO_3, SnO, γ-Fe_2O_3, β-Fe_2O_3) and the decrease of phase transformation temperatures are the consequences of oxide crystal growth peculiarities in the presence of stabilizers and the products of their thermolysis [7, 11, 12]. Usually, the formation of such phases takes place under thermoreduction of the corresponding oxides. For instance, the formation of low-temperature rutile phase is found in TiO_2 obtained by annealing of titanium hydroxide sols stabilized with acetic acid at 600 °C in air [13].

Moreover, an increased component mutual solubility and the formation of highly dispersive crystal structures with a dopant content exceeding its equilibrium concentration is inherent of complex oxide systems.

The structural features pointed above may be also caused by the presence of additives at different stages of oxide synthesis. Modifying the crystal growth is possible during crystallization of oxide structures from the stabilized sols. The role of the modifiers may be played by the stabilizing additives. They are incorporated into the sol micelle structure, and further into the structure of crystalline phases. In the case of In_2O_3, modified growth takes place both during ageing of indium hydroxide sol and under annealing of xerogels. Self-organization of nanoparticles with the formation of definite-shaped blocks takes place in colloidal solution of indium hydroxide stabilized with nitric acid. The particle dispersity may be preserved in the block structures; however, recrystallization is also possible. In the case of SnO_2, anisotropic crystal growth with the formation of needle-like and plate crystals under elevated temperatures is observed.

Thus, the addition of active components results in the alteration of i) composites dispersion, ii) system Fermi level, iii) bonding energy of metal-oxygen on the oxide surface, iv) nature and amount of adsorption centers.

It is important to note that the conditions of synthesis and, consequently, states of ions undoubtedly influence the gas-sensitive properties of simple oxides and doped oxide systems. The specific elements of structure (e.g. ions in unusual oxidation state, associates, clusters) may work as activation centers for adsorbed oxygen molecules and molecules of detected gases.

It has been shown, that red/ox-transformations of the ions in unusual oxidation state proceeding under annealing in reducing and oxidizing ambient are completely reversible [14, 15]:

$$M^{(n-1)+} - V_o \leftrightarrow M^{n+} - V_o^-.$$

It results in saving the initial high gas-sensitive activity of an oxide for long period of time. Thus, the mentioned centers may either directly participate in the detection of gases or alter the activity of oxide matrix.

Advantages of sol-gel synthesis of gas-sensitive layers are most prominent not for single oxides, but for binary oxide systems or systems «oxide-metal» (noble metals, d-metals, etc.). Their structural features provide the variety of properties of such materials.

3. GAS-SENSITIVE PROPERTIES OF OXIDES AND OXIDE COMPOSITES

3.1. Ceramic and thick film sensors

Most of metal oxide based sensors (In_2O_3, SnO_2) are characterized by low selectivity to different gases in gas mixtures; the sensitivity of these sensors is also unsuitable.

As it was established in the literature, most efficient ways to improve both selectivity and sensitivity of such sensors are: i) variation of chemical and phase composition and fine adjusting sensing layer structure, ii) control of sensor operating temperature.

Undoped In_2O_3 possesses satisfactory sensitivity to the majority of reducing gases – hydrocarbons, CO, H_2, alcohol vapors, etc. (Fig. 2). The lack of selectivity to separate gases in gas mixtures and unsatisfactory stability at long-term operation may be pointed as deficiencies of In_2O_3-sensors. To remove these disadvantages active dopants are added into In_2O_3. The addition of Ni^{2+} ions (1–5 wt % NiO) decreases In_2O_3 sensitivity to reducing gases (CH_4, H_2, C_2H_5OH, CO), but in different degree (Fig. 3) [16]. In_2O_3–NiO sensors remain satisfactory sensitive to CO at comparatively low working temperatures (200–300 °C), but become insensitive to other gases, first of all, to CH_4.

In_2O_3–Au sensors are characterized by high sensitivity to CO and independence of sensitivity on humidity. They are selective to CO in the presence of hydrocarbons at definite operating conditions.

Doping of In_2O_3 with Pt increases In_2O_3 sensitivity to low concentrations of NH_3. In_2O_3–Pt sensors allow to detect NH_3 at 1/2 threshold level (Fig. 4) [17].

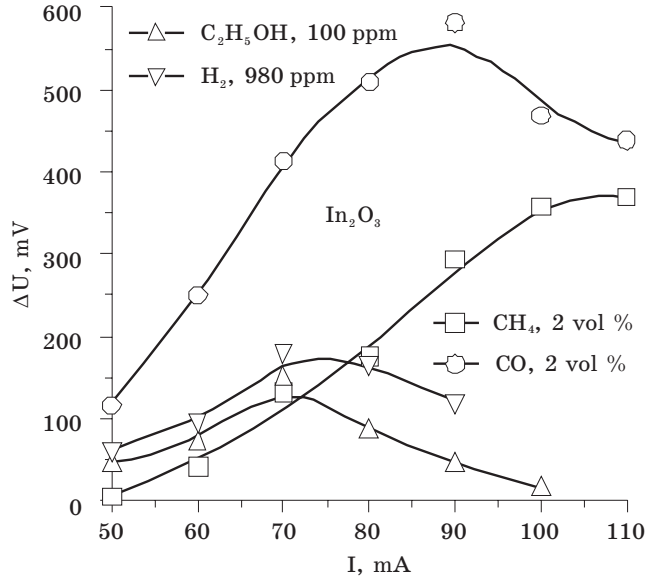

Fig. 2. Responses (ΔU) of ceramic In_2O_3 sensors vs. operating current (I)

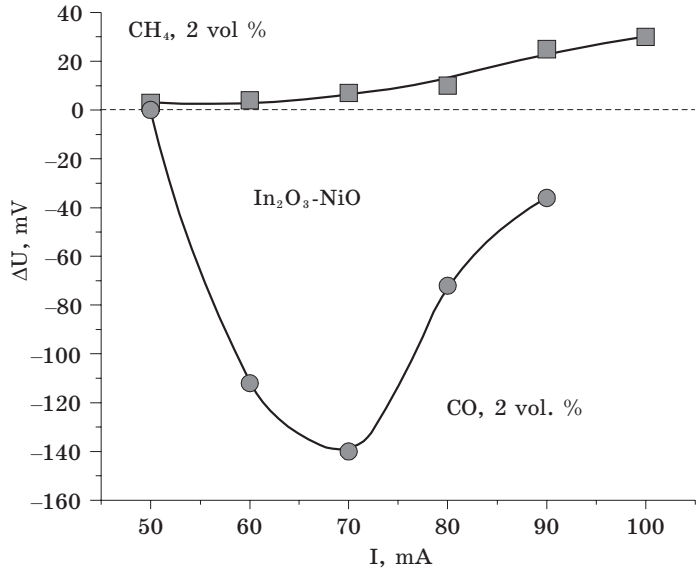

Fig. 3. Responses (ΔU) of In_2O_3–NiO ceramic sensors to CH_4 and CO vs. operating current (I)

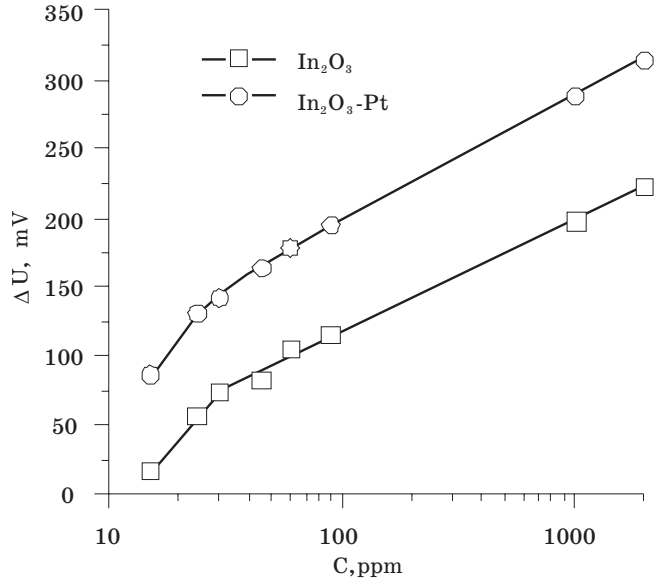

Fig. 4. Responses (ΔU) of ceramic In_2O_3 and In_2O_3–Pt sensors vs. NH_3 concentration (C)

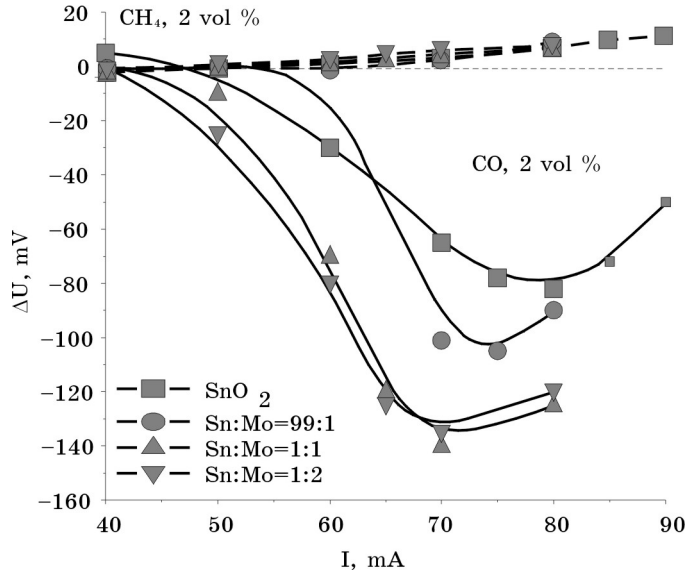

Fig. 5. Responses (ΔU) of SnO_2 and SnO_2–MoO_3 ceramic sensors to CH_4 and CO vs. operating current (I)

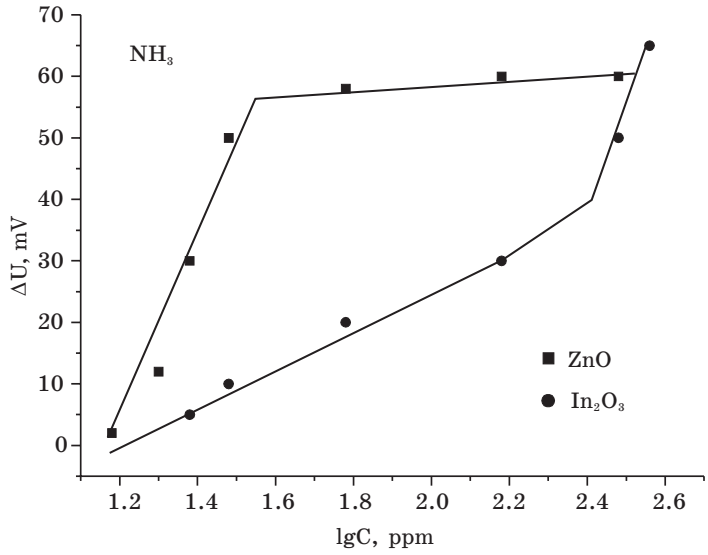

Fig. 6. Comparison of In_2O_3 and ZnO ceramic sensor behavior in NH_3 ambient

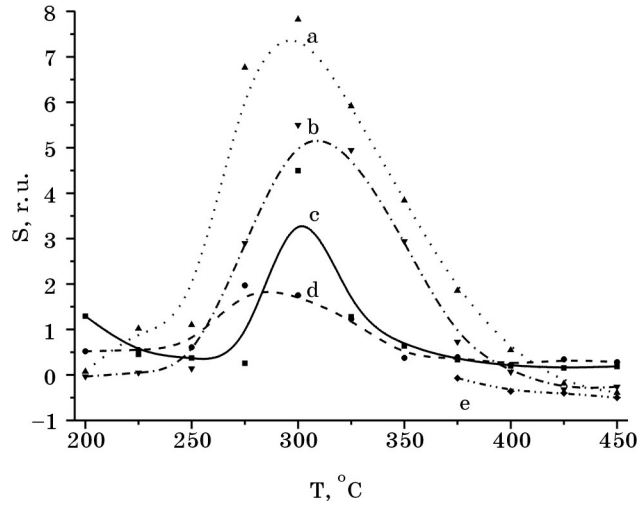

Fig. 7. Temperature dependent responses (S) to C_2H_5OH (0.025 ‰) of thick film sensors: a – α-Fe_2O_3–SnO_2 (Fe:Sn = 9:1), b – α-Fe_2O_3–SnO_2 (Fe:Sn = 1:1), c – SnO_2, d – α-Fe_2O_3, e – Fe_2O_3–SnO_2 (Fe:Sn = 1:9)

Undoped SnO_2 is characterized by unsatisfactory sensitivity to reducing gases. Therefore, gas-sensitive layers usually consist of doped tin oxide. It was found that SnO_2–Sb_2O_3–Pd sensors [18] are the most suitable for practical use. Such sensors possess gas-sensitive characteristics comparable with ones of In_2O_3-sensors. SnO_2–Sb_2O_3–Pd sensors are the most useful for detection of high concentrations of CH_4. In addition, these sensors are sensitive to formaldehyde.

The most favorable properties – threshold sensitivity levels, response values, response times – are inherent to SnO_2–In_2O_3 sensors (SnO_2:In_2O_3 = 65:35) [19].

Ceramic SnO_2–MoO_3 sensors possess the properties, which are very similar to the properties of In_2O_3–NiO sensors. At low temperatures, SnO_2–MoO_3 sensors are sensitive to CO and insensitive to hydrocarbons (Fig. 5) [20].

ZnO ceramic sensors appear to be selective when analysis of NH_3 is mentioned. They are insensitive to CH_4, CO and C_2H_5OH at temperatures optimal for NH_3 detection (Fig. 6) [21].

Fe_2O_3–SnO_2 thick film sensors demonstrate considerable activity with regards to alcohols. Thus, the highest response to ethanol shows α-Fe_2O_3–SnO_2 (9:1) nanocomposite (Fig. 7). Sensitivity of simple oxides are rather low. And the α-Fe_2O_3–SnO_2 (1:9) sample we failed to measure because of its extremely high resistance.

3.2. Thin film sensors

Thin film sensors based on simple oxides are characterized by rather low sensitivity to CO, CH_4. However, they are sensitive to O_3, NO_2 and C_2H_5OH [22-25].

With regard to the maximum response towards NO_2, the oxide films can be placed in the following consequence:

$$Fe_2O_3 > In_2O_3 > SnO_2 > MoO_3.$$

The film sensitivity depends essentially on the oxide synthesis condition and the presence of various additives (In_2O_3–MoO_3, In_2O_3–NiO, SnO_2–Fe_2O_3). Addition of a second component to the base oxide influences essentially its electrical parameters and gas sensitivity. The response of sensors of various chemical compositions to NO_2 has compared in the Table 5.

In_2O_3 thin films are almost insensitive to reducing gases [22]; meanwhile, they are highly sensitive to oxidizing gases, such as O_3 and NO_2. Addition of metal of variable valency (Ni, Mo, Fe) to In_2O_3 leads to the considerable increase of its sensitivity to NO_2 (Fig. 8). Maximum response values to NO_2 show Fe_2O_3-containing composites.

Depending on structural features of Fe_2O_3–In_2O_3 composite, the latter demonstrates prevalent sensitivity either to O_3 or NO_2. Thus, γ-Fe_2O_3–In_2O_3(9:1)/In_2O_3 sensor shows high response in the O_3 ambient at 135 °C, while its sensitivity to NO_2 at the same temperature is negligible (Figs. 9 a, b). In contrast, α-Fe_2O_3–In_2O_3(9:1)/In_2O_3 sample shows good response to NO_2 in the temperature range 50–100 °C together with rather low one to O_3. These distinctions, observed in the behavior of both composites, can be used for selective analysis of O_3 and NO_2 in gas mixture.

Generally, the sensitivity of In_2O_3 and SnO_2 films to O_3 is lower in comparison with their sensitivity to NO_2 [4, 21] In contrast, Fe_2O_3–In_2O_3 layers are characterized by higher sensitivity to O_3 than to NO_2. Moreover, the indicated compositions show better NO_2 detection performance than the previously investigated thin film sensors based on In_2O_3–NiO [23] and In_2O_3–MoO_3 [22]. Thus, γ-Fe_2O_3–In_2O_3 (9:1) and α-Fe_2O_3–In_2O_3 (9:1) composites prepared via Fe^{2+} precursor and supplied with preliminary deposited In_2O_3 sub-layer are characterized by high sensitivity to O_3 and NO_2 over a low temperature range (70–135 °C) [26], as it is reported in the Figs. 9 a, b.

Table 5

Overview of gas-sensitive (NO_2, 1 ppm) and structural characteristics of the different oxides

Sensor	S, r.u.	T, °C	Phase Composition
In_2O_3	30	150	*C*-In_2O_3
In_2O_3–NiO (99:1)	40	150	*C*-In_2O_3, H-In_2O_3
In_2O_3–NiO (95:5)	0,5	200	*C*-In_2O_3, H-In_2O_3
In_2O_3–MoO3 (9:1)	35	250	*C*-In_2O_3
Fe_2O_3	350	100	γ-Fe_2O_3
In_2O_3–Fe_2O_3 (1:1)	1150	70	*C*-In_2O_3, γ-Fe_2O_3
SnO_2	15	100	*T*-SnO_2
MoO_3	5	200	*R*-MoO_3
SnO_2–MoO_3 (99:1)	5	150	*T*-SnO_2
SnO_2–MoO_3 (3:1)	1	250	*T*-SnO2
SnO_2–Fe_2O_3 (1:1)	–2	100	*T*-SnO_2

Investigating the gas-sensitive behavior of SnO_2 and SnO_2–Mo thin films one can observe the opposite influence of Mo additive on the sensitivity of the sensors to the different gases (Table 6). By controlling MoO_3 concentration in SnO_2–MoO_3 thin films, we achieved a selective detection of both NO_2 and O_3. Thus, SnO_2-MoO_3 (Sn:Mo = 3:1) thin films are insensitive towards gaseous species like CO, CH_4, NO_2, O_3; however, they are extremely sensitive to ethanol. SnO_2–MoO_3 (Sn:Mo = = 99:1) composite is selective to ozone at 400 °C.

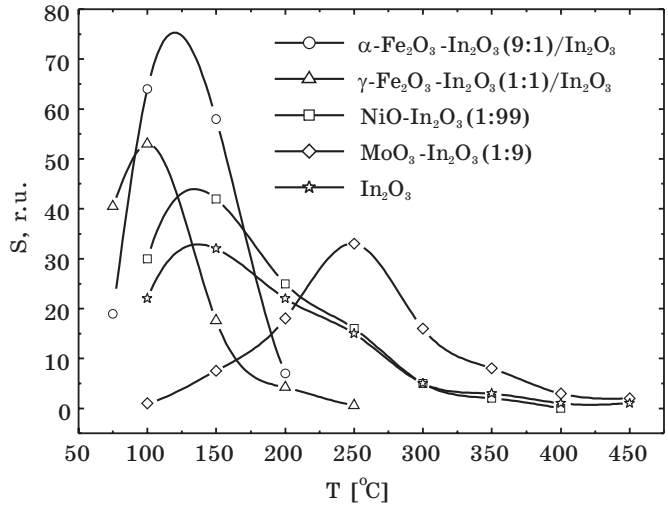

Fig. 8. Comparison of sensitivity of In_2O_3 based sensors doped with oxides of different metals to 1 ppm NO_2

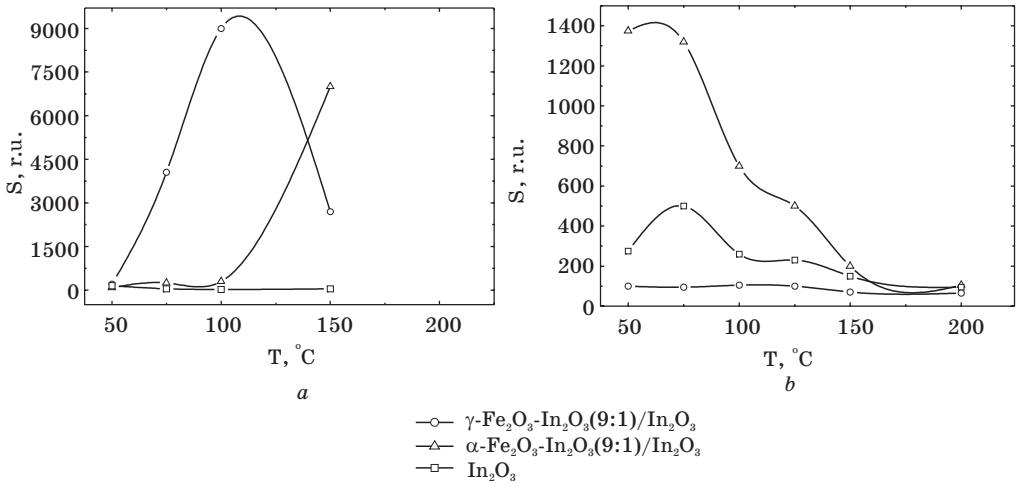

Fig. 9. Temperature-dependent responses (*S*) of In_2O_3-based sensors to oxidizing gases: *a* – 200 ppb O_3, *b* – 5 ppm NO_2

In contrast, the sensitivity to NO_2 and CO is suppressed in the presence of molybdenum. As is in the case of ethyl alcohol, the effect correlates with the content of molybdenum in the sample – the higher the content of Mo, the lower the sensor responses to CO and NO_2. Note, that in the case of CO, slight shift of the maximum sensitivity to lower temperatures was also observed.

Table 6

Gas-sensitive properties of SnO_2 and SnO_2–MoO_3 thin film sensors to different gases

Detected gas	S, r.u.		
	O_3, 175 ppb	C_2H_5OH, 500 ppm	NO_2, 1 ppm
$T_{oper.}$, °C	400	300	100
SnO_2	1	10	20
SnO_2–MoO_3 (99:1)	40	50	4
SnO_2–MoO_3 (3:1)	1	85	1

SnO_2–Pd thin film sensors [3] allow selective detection of single components (CO, NO, CH_4) in complex gas mixtures at different operating temperatures: NO at 185 °C, CO at 260–330 °C, CH_4 at 480–560 °C (Figs 10, 11). Note, that selective properties are exclusively characteristic of sol-gel obtained SnO_2–Pd sensors.

Fig. 12 clearly demonstrates the fact that the sensors based on single Fe_2O_3 and In_2O_3 layers have practically the same response values to ethanol, but they slightly differ regarding the optimal operating temperature. The sensors based on γ-Fe_2O_3/In_2O_3 heterostructure (bi-layer sensors) are characterized by significantly higher sensitivity to ethanol, than the single-layer (γ-Fe_2O_3, In_2O_3) ones. In this case, In_2O_3 sub-layer not only provides the sufficient γ-Fe_2O_3/In_2O_3 film conductivity, but it has a clear influence on the sensor sensitivity.

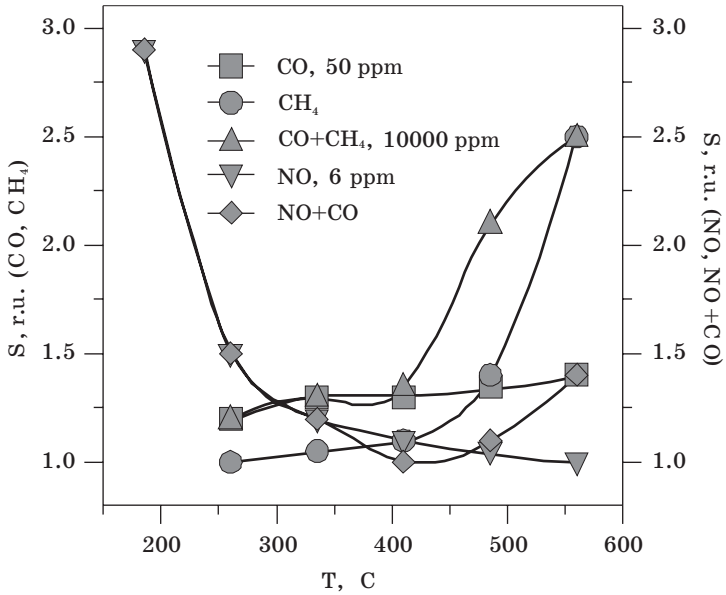

Fig. 10. SnO_2–Pd sensor responses (*S*) to CO (10 ppm), CH_4 (10000 ppm), NO (6 ppm), CO + CH_4 and CO + NO mixtures vs. operating temperature (*T*)

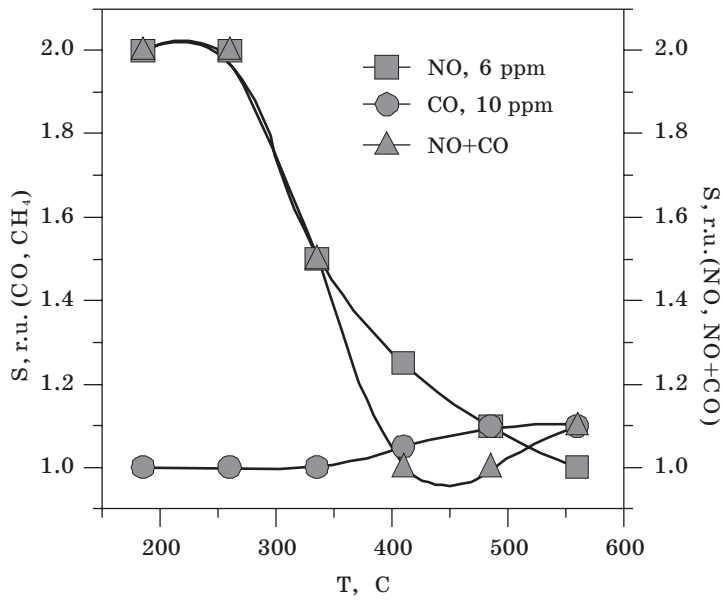

Fig. 11. SnO_2 sensor responses (*S*) to CO (10 ppm), NO (6 ppm) and CO + NO mixture vs. operating temperature (*T*)

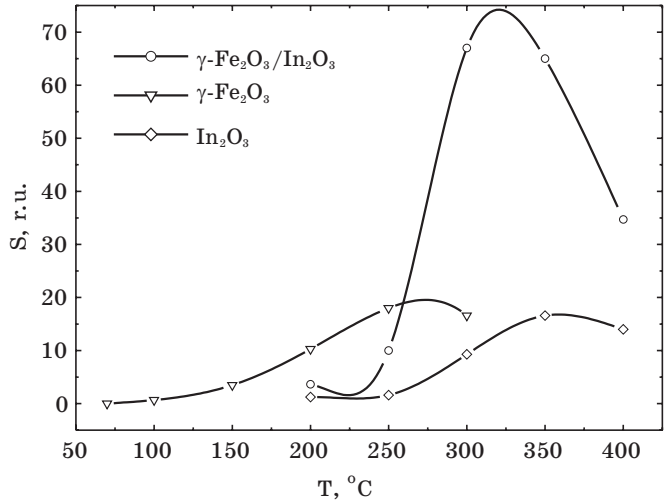

Fig. 12. Temperature-dependent responses (S) of In_2O_3 and Fe_2O_3 thin film sensors to C_2H_5OH (100 ppm)

The addition of In_2O_3 (10 % mol.) to γ-Fe_2O_3 layer leads to decrease of the γ-Fe_2O_3/In_2O_3 sensor response to ethanol (Fig. 13). According to the XRD data, γ-Fe_2O_3–In_2O_3 (9:1) composite has the structure of In^{3+} in γ-Fe_2O_3 lattice solid solution; certain amount of C-In_2O_3 phase also presents. On the contrary, further increasing In_2O_3 content within γ-Fe_2O_3 layer of γ-Fe_2O_3/In_2O_3 structure up to 50 % mol. causes abrupt rising of its sensitivity, which even overwhelms the sensitivity of γ-Fe_2O_3/In_2O_3 sample.

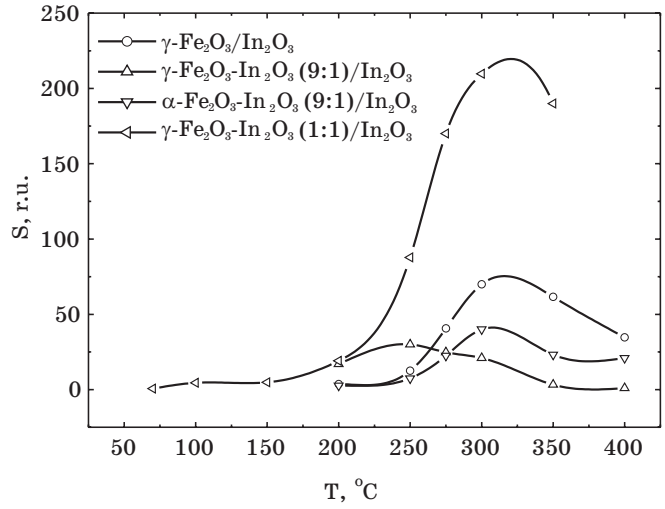

Fig. 13. Temperature-dependent responses (*S*) of In_2O_3–Fe_2O_3 bi-layer thin film sensors to C_2H_5OH (100 ppm)

In comparison with γ-Fe_2O_3–In_2O_3 (9:1) sample, γ-Fe_2O_3–In_2O_3 (1:1) one probably consists of two highly dispersive phases with great phase interface. From the XRD data of the sample it is difficult to determine exactly phase composition of the sample because of the similarity of γ-Fe_2O_3 and C-In_2O_3 crystal lattices. The growth of γ-Fe_2O_3–In_2O_3 (1:1) dense layer is due to the formation of numerous bonds between the oxide particles within this composite.

Moreover, Fe_2O_3–In_2O_3/In_2O_3 sensor sensitivity strongly depends on the crystal structure of the active layers, in particular, Fe_2O_3 phase. There are two possible Fe_2O_3 phases suitable under operating temperatures used – γ-Fe_2O_3 and α-Fe_2O_3. In the case of the pure γ-Fe_2O_3, the response achieves its maximum value at lower temperatures (250 °C), than in the case of α-Fe_2O_3 (300 °C). When methanol detection is considered, one can observe the same regularities inherited to ethanol, excepting the lower response. γ-Fe_2O_3/In_2O_3 and Fe_2O_3–In_2O_3(1:1)/In_2O_3 thin film sensors are essentially more sensitive than SnO_2–MoO_3 ones which are known to be extremely selective regarding ethanol (Table 7).

Table 7

Maximum response values of thin film sensors of various composition to ethanol (500 ppm)

Sensor	S_{max}, r.u.	T, °C
In_2O_3	15	350
γ-Fe_2O_3/In_2O_3	165	300
SnO_2	30	400
SnO_2-MoO_3	80	300

It is important to note that all double-layer sensors are much more sensitive towards alcohol (C_2H_5OH, CH_3OH) vapors than single-layer In_2O_3 and Fe_2O_3 samples; the maximum response is showed by γ-Fe_2O_3/In_2O_3 composite. Fe_2O_3-containing films are insensitive to O_3 and NO_2 over the temperature range of the most efficient ethanol detection (250–400 °C). At the same time, their sensitivity regarding ethanol is negligible at 50–150 °C when O_3 and NO_2 interaction with oxide surface has the maximum value. An increase of the In_2O_3 content within Fe_2O_3–In_2O_3 composite up to 50 % (mol.) leads to the growth of the sensor responses both to NO_2 and ethanol.

According to the responses to various gases, the sensing layers can be placed as follows:

O_3: γ-Fe_2O_3–In_2O_3/In_2O_3 > γ-Fe_2O_3/In_2O_3 > α-Fe_2O_3–In_2O_3/In_2O_3 > In_2O_3
NO_2: α-Fe_2O_3–In_2O_3/In_2O_3 > γ-Fe_2O_3/In_2O_3 > In_2O_3 > γ-Fe_2O_3–In_2O_3/In_2O_3
CO: γ-Fe_2O_3/In_2O_3 > γ-Fe_2O_3–In_2O_3/In_2O_3 ≥ α-Fe_2O_3–In_2O_3/In_2O_3 > In_2O_3
Alcohol: γ-Fe_2O_3/In_2O_3 > α-Fe_2O_3–In_2O_3/In_2O_3 > γ-Fe_2O_3–In_2O_3/In_2O_3 > In_2O_3

Referring to the results of functional and structural investigations, one can recommend a series of Fe_2O_3–In_2O_3 samples with different structure and phase composition to be used as advanced materials for O_3, NO_2 and C_2H_5OH detection. The particular compositions, dispersion and structural and phase features are listed in the Table 8.

Table 8

The most promising gas-sensitive materials recommended for fabrication of highly selective sensors and their structural peculiarities. Temperature of annealing 300 °C

Sensor	T, °C	Detected Gas	Gas conc., ppm	Phase Composition	Grain Size, nm
γ-Fe_2O_3–In_2O_3(9:1)/In_2O_3 via $Fe(OH)_2$, mixing	135	O_3	0.06	γ-Fe_2O_3 C-In_2O_3	25 25
α-Fe_2O_3–In_2O_3(9:1)/In_2O_3 via Fe(II), co-precipitation	70–100	NO_2	0.5	α-Fe_2O_3 (anisotropic)	8 × 15
γ-Fe_2O_3/In_2O_3 via $Fe(OH)_2$	250	C_2H_5OH	50	γ-Fe_2O_3	25–30
γ-Fe_2O_3–In_2O_3(1:1)/In_2O_3 via Fe_3O_4, mixing	70–100	NO_2	0.5	C-In_2O_3	7–8
	300	C_2H_5OH	50	γ-Fe_2O_3	5
α-Fe_2O_3–In_2O_3(1:1)/In_2O_3 via $Fe(OH)_3$, mixing	300	C_2H_5OH	50	Amorphous C-In_2O_3	– 8
α-Fe_2O_3–In_2O_3(9:1)/In_2O_3 via $Fe(OH)_3$, mixing	300	C_2H_5OH	50	Amorphous	–

4. REGULARITIES OF NO_2, O_3 AND C_2H_5OH DETECTION

On the basis of the obtained results we made an attempt to find the correlations between structural features of different oxide systems and their gas-sensitive behavior.

4.1. Nitrogen dioxide

Two models of conductivity changes should be considered at the interaction of metal oxides with oxidizing gas molecules. The first model deals with adsorption in molecular form and corresponding surface band bending, whereas the second model takes into account chemical interactions leading to changes of oxide stoichiometry and charge carrier concentration. In the case of sol-gel obtained highly defective metal oxide systems, the second model looks preferable.

The model of NO_2 detection by thin film In_2O_3-sensors has been described elsewhere [27]. The model explains change of In_2O_3 films conductivity in terms of surface band bending due to molecular adsorption of O_2 and NO_2. It is supposed that In_2O_3 film conductivity is determined by the presence of adsorbed oxygen, which plays the role of electron acceptor and is in equilibrium with In_2O_3 surface defects. Molecular adsorption of NO_2 upsets this equilibrium and creates additional acceptor levels. The centers of O_2 and NO_2 adsorption on indium oxide are electron defects of structure, namely In^{2+} and *F*-centers. The increase of In_2O_3 sensitivity to NO_2 at doping with Ni^{2+} can be explained by an increase of In^{2+} and oxygen vacancy concentration in $In_{2-x}Ni_xO_3$ solid solution structure. The generation of In^{2+} ions is due to the following process:

$$In^{3+} + Ni^{2+} > In^{2+} + Ni^{3+}.$$

It is known that band mechanism of charge transfer occurs in In_2O_3 at comparatively low temperatures (T<550 °C) [8]. At low temperature electrons caused by the presence of In^{2+} and In^{+} ions in indium oxide are delocalized and transfer to conductivity band formed by overlapping of In 5s-orbitals. Broadening of In^{2+} ESR signals and absence of hyper-fine structure lines in ESR spectra of nonstoichiomertic In_2O_3 indicate the delocalization of electrons [7]. High mobility of electrons in In_2O_3 at low temperature is provided by easy electron exchange process between In^{2+} and In^{+} ions: $2In^{2+} \leftrightarrow In^{3+} + In^{+}$. Lower conductivity of $In_{2-x}Ni_xO_3$ solid solution as compared to undoped In_2O_3 may be caused by decreasing of free carrier mobility and change of conductivity mechanism.

The deviation from the band charge transfer mechanism is very possible for In_2O_3-based solid solutions [8, 16, 23]. The charge transfer in In_2O_3–Ni^{2+} system is probably occurs not only through In–O–In but also through In–O–Ni–O–In chains. The participation of Ni^{2+}/Ni^{3+} ions in charge transfer decreases the rate of electron exchange in In_2O_3–Ni^{2+} as compared to In_2O_3. It is known that d-orbitals of nickel are localized at separate ions and overlap insignificantly.

When NO_2 is detected by In_2O_3-sensors, not only NO_2 adsorption and related In_2O_3 conductivity changes, but also the possibility of chemical interaction between indium oxide and NO_2 and stipulated change of defect concentration should be taken into account [22, 27]. NO_2 is the strong oxidizing agent. It is known that NO_2 dissotiatively chemisorbed at semiconductor oxide surface oxidizes structure defects – partially reduced ions (i.e. In^{2+}) and oxygen vacancies, and causes the formation of atomic oxygen at In_2O_3 surface. The appearance of additional oxygen at In_2O_3 films after treatment with $NO_2 + O_2$ mixture has been found by means of XPS [22]. At comparatively low temperatures NO_2 chemisorption occurs mainly at partially reduced centers (In^{2+}) with the formation of surface complexes: In^{2+}–O–N=O. The oxidation process $In^{2+} \rightarrow In^{3+}$ is accompanied by tearing oxygen atom off from chemisorbed NO_2 molecule in surface complex. Under these conditions N–O bond breaking energy must be compensated by In–O bonding energy. Such process is energetically profitable in the case of either In^{2+} or Ni^{2+} [27]. Note, that O–O bonding energy (480 kJ mol^{-1}, O_2) is higher than N–O one (292 kJ mol^{-1}, NO_2). Thus, the oxidation of In_2O_3 and In_2O_3–Ni^{2+} surface in O_2 ambient requires higher temperature than in $NO_2 + O_2$ ambient. It may provide the detection of low NO_2 concentration in O_2 presence at low operating temperatures. The possibility of chemical reaction between indium oxide and NO_2 is indicated by slow recovery of In_2O_3-based thin film sensors at detection of NO_2.

The proceeding of oxidation process when interacting of TiO_{2-x} with NO_2 has been proved by Iuengar et al. [28] They found the sample weight changes, disappearance of Ti^{3+} ESR signal and appearance of NO and N_2O_3 species in gas phase after NO_2 adsorption-desorption cycle at TiO_{2-x} sample. Capehart and Chang [29] proved that SnO_{2-x} conductance changes under NO treatment is not due to surface band bending but due to SnO_{2-x} oxidation accompanying by decrease of oxygen vacancy bulk concentration.

In the case of Mo-containing oxide systems, $Mo^{(5+\delta)+}$–$O_n^{\delta-}$ complexes appear to be active centers of gas adsorption. The formation of the mentioned complexes is confirmed by XPS study of In_2O_3–MoO_3 composites exposit to NO_2 vapors (Fig. 14).

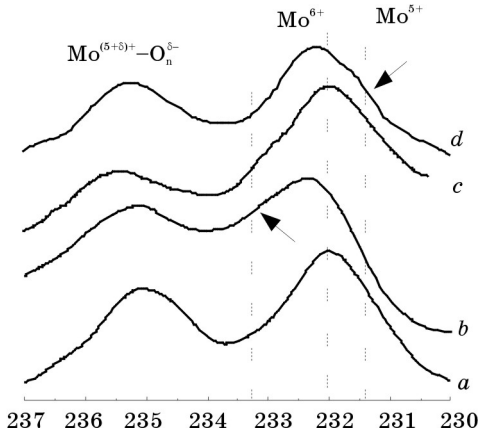

Fig. 14. Mo 3d X-ray core level in XPS spectra of In_2O_3–MoO_3 films annealed: *a* – in air (400 °C, 1 h), *b* – in NO_2 (200 °C; 0.5 h), *c* – in vacuo (200 °C; 0.5 h), *d* – in air (700 °C, 1 h)

Composites prepared by using sol-gel technology are characterized by increased solubility of the additives and the formation of crystal structures with dopant content exceeding its equilibrium concentration. The presence of the second oxide component retards the crystallization and the particle growth of base oxide (In_2O_3–NiO, ZnO–MoO_3), and it favors the stabilization of amorphous (SnO_2–MoO_3, SnO_2–Fe_2O_3) and metastable phases. In_2O_3 sample doped with Ni^{2+} and Mo^{VI} ions results in an increase of In_2O_3 nonstoichiometry degree and stabilization of In^{2+} and *F*-centers, which are activation points of NO_2 gaseous species.

The indicated structural peculiarities of oxide systems explain clearly the observed difference in NO_2 detection of oxide nanocomposites like In_2O_3–NiO, In_2O_3–MoO_3, SnO_2–MoO_3.

As it was noted above, Fe_2O_3–In_2O_3 (1:1) sample demonstrates the highest sensitivity to NO_2 as compared to other systems (see Fig. 8, Table 5). The special composite structure, whose important parameters are represented by phase composition, dispersion, morphology of particles and manner of their coalescence with the formation of numerous bonds provides the optimum set of adsorption and catalytic properties. According to the XRD data, Fe_2O_3–In_2O_3 (1:1) composite is a heterogeneous system; it consists of Fe^{3+} in In_2O_3 lattice solid solution and γ-Fe_2O_3 phases. It is important to take into consideration that In_2O_3 and Fe_2O_3 oxides have a similar crystal structure. The solubility of Fe_2O_3 in In_2O_3 lattice essentially exceeds the equilibrium value; it provides a very close contact between the particles of two phases and thereby facilitates the charge transfer. Sufficient film electroconductivity is also due to the lacy framework of the phase based on In_2O_3.

In order to elucidate the origin of very high sensitivity of Fe_2O_3–In_2O_3 nanocomposites prepared by both co-precipitation and mixing of Fe(II) and In(III) hydroxides the careful structural examination of the studied samples was carried out.

As it was found from the XRD studies, all the samples appear to be nanosized. The composites annealed at 300 °C differ by phase composition that depends on synt-

hesis conditions. Thus, Fe_2O_3–In_2O_3 species obtained by Fe(II) and In(III) hydroxide mixing contain γ-Fe_2O_3, which is metastable at room temperature. Structural peculiarities of the mentioned modification of Fe_2O_3 such as readiness of $Fe^{3+} \leftrightarrow Fe^{2+}$ charge transfer and high conductivity as well as differentiation between the functions of receptor and transducer between different phases (Fe_2O_3 and In_2O_3) provides high performance of Fe_2O_3–In_2O_3 sensors. Co-precipitation of Fe(II) and In(III) hydroxides leads to the crystallization of highly dispersive α-Fe_2O_3 which is the most thermodynamically stable Fe_2O_3 phase. ESR data give evidence that the mentioned composites contain Fe–O–Fe associates, $(FeO)_x$ clusters or micro-inclusions of Fe_2O_3 amorphous phase. Fe(III) ions are characterized by cubic symmetry of coordination environment. The very areas of poorly crystallized (or amorphous) phase are active in gas adsorption that follows from the increasing of the corresponding ESR signal intensity under exposure of the Fe_2O_3–In_2O_3 layers in NO_2 ambient (Fig. 15). Isolated Fe(III) ions are not participating in this process.

In the case when the species is only consisted of amorphous phase, suitable value of sensing layer conductivity is not reaching. The presence of amorphous phase is essential in quantity, sufficient to provide a chemisorption of detected gas, but not making difficult the charge transfer. The later should be provided by other highly conductive phases (C-In_2O_3).

Mossbauer spectroscopy analysis of the Fe_2O_3–In_2O_3 composite of different structure and simple Fe_2O_3 oxides allowed to conclude that local crystal environment of Fe(III) ions within the co-precipitated sample prepared via Fe(II) precursor and having the structure of α-Fe_2O_3 is closer to the environment, which is typical of cubic γ-Fe_2O_3 rather than to trigonal α-Fe_2O_3 (Fig. 16, Table 9). The indicated phase consisting of three types of Fe_2O_3-centers is extremely active in gas adsorption.

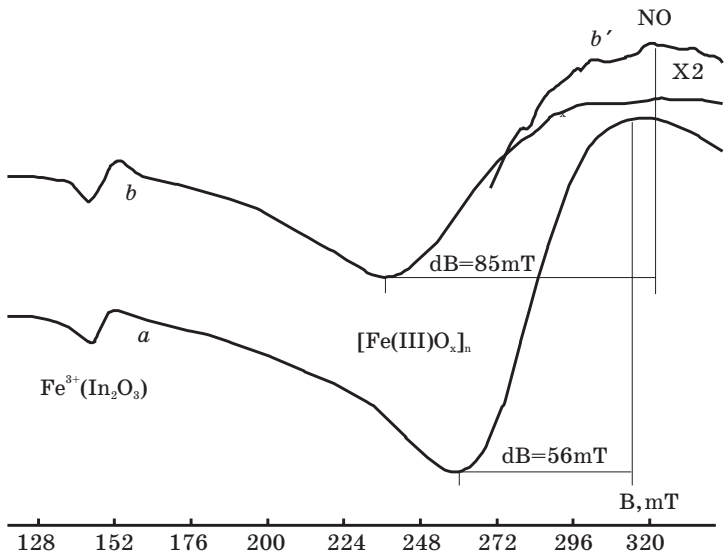

Fig. 15. ESR spectra of α-Fe_2O_3–In_2O_3 (1:1) composite, annealed at 800 °C:
a – initial, *b* – treated in NO_2 at 120 °C, 0.5 h

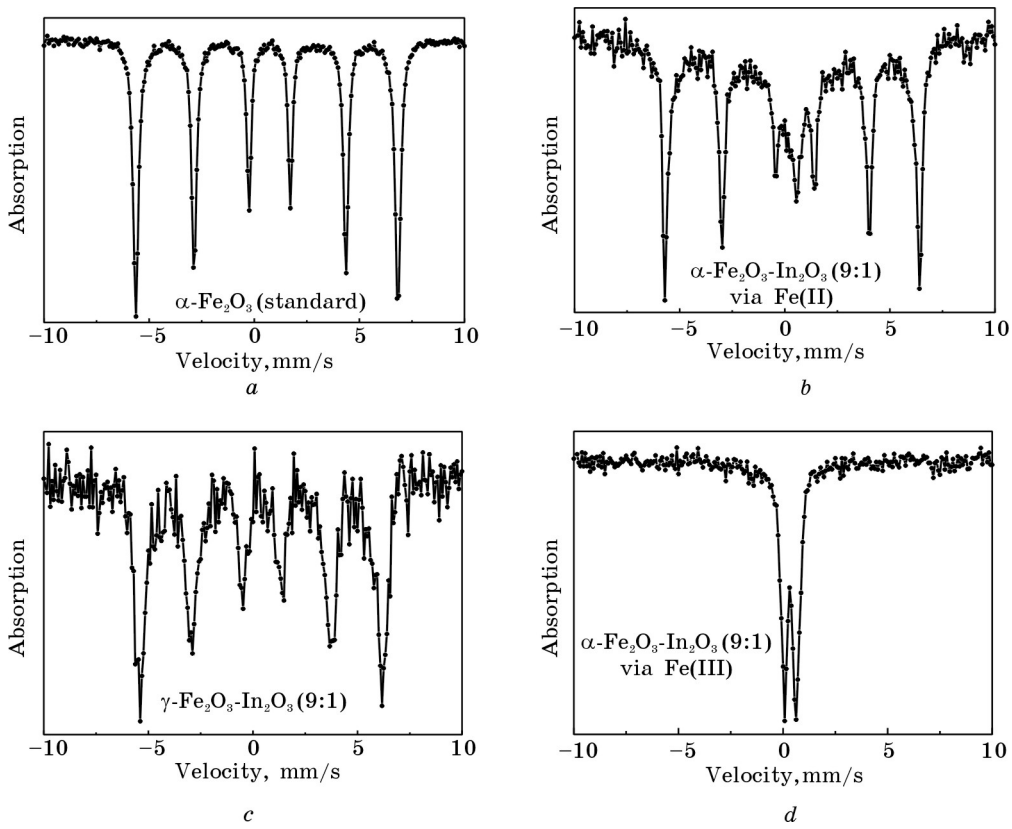

Fig. 16. Mossbauer spectra recorded from Fe-containing species at 298 K:
a – α-Fe_2O_3 standard, *b* – α-Fe_2O_3–In_2O_3 (9:1), via Fe(II),
c – γ-Fe_2O_3–In_2O_3 (9:1), *d* – α-Fe_2O_3–In_2O_3 (9:1), via Fe(III)

Table 9

Parameters of Mossbauer spectra recorded from Fe-containing samples at 298 K

Sample	δ, mm s^{-1}		Δ, mm s^{-1}	*B*, *T*
α-Fe_2O_3–In_2O_3 (9:1) (300 °C), via Fe(II)	0.38 0.53 0.22	78 % 15 % 7 %	0.08 0 0.69	50.7 0 0
α-Fe_2O_3–In_2O_3 (9:1) (300 °C), via Fe(III)	0.30		0.777	0
γ-Fe_2O_3–In_2O_3 (9:1) (300 °C)	0.33		0.02	48.6
γ-Fe_2O_3 (300 °C)	0.34		–0.03	49.1
γ-FeOOH (300 °C)	0.33		0.78	0
α-Fe_2O_3 (amorphous) (300 °C)	0.39		0.09	50.7
γ-Fe_2O_3 (standard sample)	0.34÷0.39		–0.05÷-0.1	49.8÷50.6
α-Fe_2O_3 (standard sample)	0.47 0.38		0.24 0.12	51.8 51.5

4.2. Ozone

O_3 and NO_2 are interfering gases as they both demonstrate similar chemical properties. To separate sensor signals attributed to NO_2 and O_3 transformation the following aspects should be mentioned: i) oxide materials possess unequal catalytic activity in O_3 and NO_2 decomposition process, ii) inherent distinctions in NO_2 and O_3 molecule adsorption and desorption of their decomposition products.

Thus, the sensors based on oxides which are active catalysts of O_3 decomposition (like Fe_2O_3) demonstrate maximum response at low temperature (70–100 °C). In the case of catalysts of low activity (like MoO_3, SnO_2), optimal temperature value shifts sidewise high temperatures (150–300 °C). Adsorption of O_3 is going at external side of oxide surface; meanwhile NO_2 adsorbs at pores (at internal oxide surface).

Mechanisms of O_3 detection at different temperatures can be presented by the following scheme:

At low temperature (70–100 °C)	***At high temperature (150–300 °C)***
Adsorption of O_3	
$M + O_3 \rightarrow O_2 + M–O$ (at oxide surface)	$O_3 \rightarrow O_2 + O$ (in vapor phase)
$2M–O + O_3 \rightarrow M + O_2$	$O + M \rightarrow M–O$
	$2M–O \rightarrow 2M + O_2$
Desorption of chemisorbed O_2	
$O_3 + MO \rightarrow M + 2O_2$	$2MO \rightarrow 2M + O_2$

The desorption of chemisorbed O_2 is principally different for O_3 and NO_2. It can be realized for O_3 at low temperature only through the attack of MO-intermediate by O_3 molecule. The desorption of oxygen in the case of NO_2 goes only by the second route at high temperature. The distinctions in NO_2 and O_3 optimal detecting temperature allow selective analysis of single gases in gas mixture.

4.3. Ethanol

Two ways of alcohol (for example, ethanol) molecule conversion are possible at the oxide surface – dehydrogenation and dehydration:

$CH_3CH_2OH \rightarrow CH_3CHO + H_2$ (dehydrogenation) (1)
$CH_3CH_2OH \rightarrow C_2H_4 + H_2O$ (dehydration) (2)

According to the literature data, dehydrogenation (1) mainly occurs at the oxide surfaces with basic properties, and requires higher reaction temperatures in comparison with dehydration. Dehydration (2) is a typical example of acid basic reactions, and dominates at decreased temperatures and at acid surfaces. According to the results of Kohl [30] and Yamazoe et al. [31], the detection of ethanol at SnO_2 proceeds through dehydrogenation route. Ethanol is adsorbed at surface tin atoms, and the process goes with the elimination of H from OH-groups forming acetaldehyde CH_3CHO. MoO_3 is an example of typical acid catalyst [32]. However, the acidic properties of MoO_3 become apparent only if the bulk molybdenum oxide phase forms. The process of the alcohol

dehydration on MoO_3 proceeds by the classical acid-basic mechanism through the formation of carbonium ions. It is caused by the stabilization of hydrogen atoms and hydroxyl groups in the molybdenum oxide structures at the stage of their formation. These stabilized spices play the role of catalytic centers [33].

In the case of multi-component oxide systems, the complex dependencies in the alcohol conversion can be observed. The appropriateness of the change of catalytic properties in the acid-basic reactions is often opposite those in the red/ox reactions. In the certain cases, the addition of basic oxides (e.g. La_2O_3) to SnO_2 increases, and the addition of acid oxides (MnO_2) decreases the sensitivity to ethanol. However, as we observe in the case of SnO_2–Mo, the acid MoO_3 increases the sensitivity to ethanol and decreases the detection temperature. The addition of acid catalyst (e.g. Al_2O_3) gives a similar effect [34]. High sensitivity of SnO_2–Al_2O_3 to ethanol is due to bifunctional catalytic properties. Al_2O_3 catalyses dehydration of ethanol with the formation of ethylene C_2H_4 adsorbed at the SnO_2 surface. When added to TiO_2, WO_3, also known as acid catalyst, enforces dehydrogenation and suppresses dehydration of ethanol [35].

As it was found out by our group, the detection of alcohols using semi-conducting oxides goes by oxidizing dehydrogenation pathway:

$$C_2H_5OH + 1/2\ O_2 \rightarrow CH_3CHO + H_2O \text{ (oxidizing dehydrogenation)} \qquad (3)$$

The oxidizing dehydrogenation of alcohol (3) is heterolytic catalytic reaction. The process involves both reductive-oxidative and acid-base steps. In particular, alcohol molecule adsorption at metal cation, which plays a role of Lewis centre, is related to acid-base reaction.

The relative measure of oxide activity in the oxidation reactions can be oxygen-oxide surface bonding energy. In fact, the less the energy of oxygen atom isolation from an oxide surface, the higher the oxide oxidizing ability. The reactivity of oxides in acid-base reactions depends on the electronegativity of cations M^{n+}: $\chi = \chi_o(2n+1)$, where χ_o – Pauling's electronegativity, n – ion charge. The electronegativity can be used as the measure of Lewis acid site activity. The adsorption of alcohol molecules at Lewis sites is going with great output. Complete oxidation of intermediate products is possible at the surface of the oxide, which is characterized by small values of M–O binding energy and electronegativity. According to the electronegativity (χ) increasing, the studied oxides can be placed as follows (Table 10):

$$In_2O_3 < Fe_2O_3 < SnO_2 < MoO_3.$$

But in the general case, reductive-oxidative and acid-base properties of oxide surface may not correlate.

Thus, detection of ethanol using oxide materials, where metal is greatly electronegative (MoO_3) is not accompanying by complete oxidation of intermediates, but is characterized by striking selectivity.

In the range of considerable M–O bonding energy values, donor-acceptor interaction between alcohol molecules and $M^{m+}O^{2-}$ species become clearly apparent. Oxides containing Mo (VI) cations, which are strong Lewis acids, are very active. In fact, low bonding energy and strong basic properties of an oxide promote further oxidation of intermediates of alcohol molecule transformation (Fig. 17), thereby increasing the corresponding sensor response values.

Table 10

The metal-oxygen binding energy for some oxides

Metal Oxide	E_{M-O}, kcal/g per atom	Electronegativity, r.u.
MoO_3	91	30.55
SnO_2	70	17.64
Fe_2O_3	56	13.72
In_2O_3	–	12.46

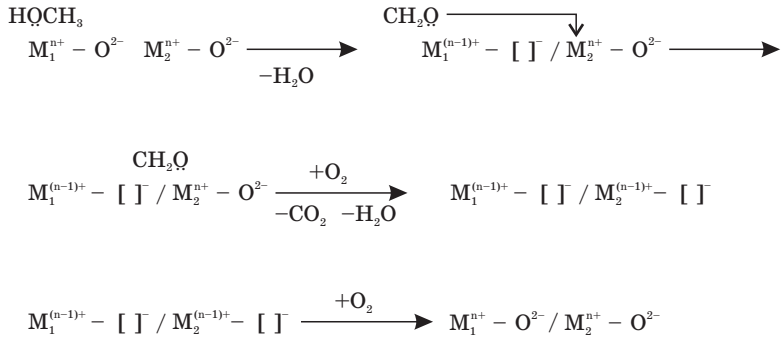

Fig. 17. The scheme of alcohol oxidation process at oxide phase interface by the example of methanol (CH_3OH) oxidation

The oxides, which are characterized by the possibility of metal ion reduction without oxide phase state modification, have the greatest ability to promote oxidizing dehydrogenation processes. For instance, such oxides as MoO_3, In_2O_3 and Fe_2O_3 are inclined to facile the changing of metal ion oxidation state: Mo(VI) ↔ Mo(V), In(III) ↔ In (II), Fe(III) ↔ Fe(II), while oxide phase remains original.

The sensors based on heterojunction oxide structure show considerable response to alcohol (ethanol, methanol) vapors. The heterojunction between an oxide and solid solution phases appears to be very active in both adsorption and oxidation of alcohol. The presence of two types of centers possessing different reductive-oxidative and acid-base properties, and participating in the processes of the alcohol molecule transformation is essential requirement to achieve high sensor response when alcohol detection is considered. The centers of one type can suitably participate in adsorption-desorption processes of alcohol molecules, whereas complete oxidation of intermediates effectively proceeds at the centers of another type.

As it was appeared, the experimental data regarding both catalytic and gas-sensitive properties of most of semi-conducting oxides are not in accordance with prevailing conception, asserting that the alcohol detection is predominately realized as dehydration process (2), when oxide with acidic properties are used, and as dehydrogenation (1) at base oxide surface. Thus, MoO_3 possesses strong acidic behavior. At the same time, it is one of the most efficient catalysts of methanol conversion into formaldehyde (reaction of dehydrogenation). By reason of MoO_3 high catalytic activity, it being added to SnO_2 species evokes the increasing

the corresponding sensor sensitivity towards alcohols. However, in this case, after-oxidation of formaldehyde, generated during dehydrogenation step, to form CO_2 and H_2O is impossible because of great Mo–O bond strength within MoO_3. Using this fact one can explain lesser response of SnO_2–MoO_3 sensors to ethanol in comparison with Fe_2O_3–In_2O_3 ones.

From the evidence reported one can conclude that the main process determining the efficiency of alcohol detection using semi-conducting oxides is oxidizing dehydrogenation process including both oxidation-redaction and acid-base steps. Hence, sensors based on heterojunction oxide systems and containing two types of centers show better performance.

5. CONCLUSION

As it follows from the reported data, by means of In_2O_3 and SnO_2 oxide doping and varying of their synthesis and annealing conditions it is possible to control gas-sensitive properties of the corresponding sensors. Gas-sensitivity can be varied within wide range by changing the structure of sensitive layers. Advanced materials suitable for selective detection of important gaseous species have been proposed. The material compositions, threshold gas concentration and operating temperature are listed in the Table 11.

Table 11

Sensor types, compositions and optimal conditions for selective detection of commonly determined gases

Detected Gas	Threshold concentration, ppm	$T_{oper.}$, °C	Gas-Sensitive Layer
NO_2	0.5	70–100	α-Fe_2O_3–In_2O_3, thin film
	0.2	250	MoO_3–In_2O_3 (1:9), thin film
O_3	0.06	400	MoO_3–SnO_2 (1:99), thin film
	0.045	100	γ-Fe_2O_3–In_2O_3 (9:1), thin film
	0.045	100	MoO_3–In_2O_3 (1:9), thin film
CO	200	200–250	NiO–In2O3 (1:9), ceramic
	200		MoO_3–SnO_2 (1:3), ceramic
CH_4	1000	500–550	SnO_2–Pd, thin film / ceramic
	20		SnO_2–Sb–Pd, ceramic
C_2H_5OH	50	300	γ-Fe_2O_3–In_2O_3(1:1)/In_2O_3, thin film
C_2H_5OH	50	300	γ-Fe_2O_3/In_2O_3, thin film
NH_3	15	300	ZnO, ceramic

ACKNOWLEDGMENTS

The work has been supported by international programs «INTAS» (project 2000–0066) and «COPERNICUS» (projects EASTGAS (1998-2000) and GASMOH (2000–2003).

REFERENCES

1. *Ивановская М. И.* // Избранные научные труды Белорусского университета: В 7 т. Т. 5. Химия / Отв. ред. В. В. Свиридов. Мн.: БГУ. 2001. С. 242.
2. *Orlik D. R., Ivanovskaya M.I., Bogdanov P. A.* et al. // Sensors and Actuators B. 1993. Vol. 13–14. P. 605.
3. *Орлик Д. Р., Ивановская М. И., Коль К. Д.* // Журн. аналит. химии. 1995. Т. 50, № 11. С. 1173.
4. *Gurlo A., Ivanovskaya M., Barsan N.* et al. // Sensors and Actuators B. 1997. Vol. 44. P. 327.
5. *Ивановская М. И., Браницкий Г. А., Орлик Д. Р.* и др. // Журн. неорг. химии. 1992. Т. 37. Вып. 5. С. 1147.
6. *Ivanovskaya M. I., Bogdanov P. A., Orlik D. R.* et al. // Thin Solid Films. 1997. Vol. 296. P. 41.
7. *Ивановская М. И., Богданов П. А., Гурло А. Ч.* и др. // Неорг. материалы. 1998. Т. 34, № 3. С. 329.
8. *Gurlo A., Ivanovskaya M., Pfau A.* et al. // Thin Solid Films. 1997. Vol. 307. P. 288.
9. *Ивановская М. И., Романовская В. В., Браницкий Г. А.* // Журн. физ. химии. 1994. Т. 68, № 2. С. 232.
10. *Ивановская М. И., Лютынская Е. В.* // Журн. физ. химии. 1997. Т. 71, № 10. С. 1830.
11. *Гурло А. Ч., Ивановская М. И.* // Неорг. материалы. 1998. Т. 34. № 12. С. 1466.
12. *Ивановская М. И., Лютынская Е. В., Ивашкевич Л. С.* // Журн. неорг. химии. 1998. Т. 43. № 10. С. 1716.
13. *Мальченко С. Н., Есмаиел Е., Ивановская М. И.* и др. // Неорг. материалы. 1992. Т. 28, № 7. С. 2327.
14. *Орлик Д. Р., Ивановская М. И., Браницкий Г. А.* и др. // Сб. науч. трудов: Золь-гель процессы получения неорганических материалов. Екатеринбург: УрО РАН. 1996. С. 56.
15. *Фролова Е. В., Ивановская М. И., Азарко И. И.* и др. // Докл. НАН Беларуси. 2002. Т. 46, № 2. С. 74.
16. *Ivanovskaya M., Bogdanov P.* // Sensors and Actuators B. 1998. Vol. 53. P. 44.
17. *Romanovskaya V., Ivanovskaya M., Bogdanov P.* // Sensors and Actuators B. 1999. Vol. 56. P. 31.
18. *Орлик Д. Р., Ивановская М. И., Гурло А. Ч.* // Журн. аналит. химии. 1997. Т. 52, № 1. С. 69.
19. *Bogdanov P., Ivanovskaya M.* // Proc. VIth Eur. Conf. Solid State Chem. Switzerland, Zurich. 1997. P. PA65.
20. *Ivanovskaya M., Lutynskaya E., Bogdanov P.* // Sensors and Actuators B. 1998. Vol. 48. P. 388.
21. *Гурло А. Ч., Ивановская М. И.* // Журн. физ. химии. 1998. Т. 72, № 2. С. 364.
22. *Gurlo A., Barsan N., Ivanovskaya M.* et al. // Sensors and Actuators B. 1998. Vol. 47. P. 92.
23. *Bogdanov P., Ivanovskaya M., Comini E.* et al. // Sensors and Actuators B. 1999. Vol. 57. P. 153.
24. *Ivanovskaya M., Gurlo A., Bogdanov P.* // Sensors and Actuators B. 2001. Vol. 70. № 1–2. P. 264.
25. *Ivanovskaya M., Bogdanov P., Faglia G.* et al. // Sensors and Actuators B. 2001. Vol. 70. № 1–2, P. 268.
26. *Ivanovskaya M., Kotsikau D., Faglia G.* et al. // Proc. Int. Meet. on Chemical Sensors, Boston, USA. July 7–10. 2002. P. 458.

27. *Ivanovskaya M., Bogdanov P., Faglia G.* et al. // Sensors and Actuators B. 2000. Vol. 68. P. 344.
28. *Iuengar R. D., Codell M., Turkevich J.* // J. Catal. 1967. Vol. 9. P 305.
29. *Capehart T.W., Chang S.-C.* // J. Vac. Sci. Technol. 1981. Vol. 18. P 393.
30. *Kohl D.* // Sensors and Actuators B. 1989. Vol. 18. P. 71.
31. *Yamazoe N.* // Sensors and Actuators B. 1991. Vol. 5. P 7.
32. *Крылов О. В.* Катализ неметаллами. Л.: Химия. 1967. 240 с.
33. *Mehandru S. P., Anderson A. B.* // J. Am. Chem. Soc. 1988. Vol. 110. P. 2061.
34. *Xu T.* // J. Chin. Ceram. Soc. 1993. Vol. 21. P. 192.
35. *Волькенштейн Ф. Ф.* Электронные процессы на поверхности полупроводников при хемосорбции. М.: Наука. 432 с.